NOISE VERSUS COHERENCY IN MM-WAVE AND MICROWAVE SCATTERING FROM NONHOMOGENEOUS MATERIALS

B. Kapilevich and B. Litvak

Department of Electrical and Electronics Engineering
Ariel University Center of Samaria, Ariel 44700, Israel

Abstract—Forward scattering effects have been studied and compared when nonhomogeneous medium is illuminated by coherent and quasi-noise sources operating in mm-wave and microwave ranges. Double-layers dielectric structure simulating Fabry-Perot resonator properties was employed to develop a relevant model used for comparing transmittances of both coherent and noise signals. Experiments with nonhomogeneous materials such as coal, wood chips, sand and others have proved the basic modeling predictions and the role of noise bandwidth in averaging process important for material characterizations. It was found out that efficient averaging associated with noise nature of probing signal can be reached for the relative noise bandwidth of 25% and more.

1. INTRODUCTION

Microwave, mm-wave and THz waves are widely used now for characterization a variety of materials such as solids, liquids, gases etc.. There are different microwave techniques suggested for determination complex permittivity in wide frequency range covering RF, microwaves and mm-wave bands [1]. However, most of these techniques were basically developed for characterizing homogeneous bulky materials. In the case of nonhomogeneous medium such as granular materials with arbitrary particle shaping some additional factors must be taken into consideration: the shape of particles, frequency range, polarization effects as well as coherency properties of probing signal. Various models have been introduced for predicting both forward and backward scattering effects in dense random media [2, 3]. On the other hand

theoretical and experimental studies these materials are made difficult due to the ambiguity associated with the above mentioned factors. The theoretical approaches have been basically developed well for homogeneous systems and for cases of particles of spherical and ellipsoidal shape [4, 7].

In many publications coherent electromagnetic fields are basically employed in scattering characterization of granular materials [5–7]. Also, theoretical models based on quasi-static approach [4] are widely used limiting interpretation of scattering and depolarization effects taken place in granular materials when a particle size is comparable with a wavelength. Such a situation is typical for mm-wave and THz ranges. In order to avoid polarization mismatching and coherent interference effects an incoherent noise-like illumination can be useful as reported in [8, 9]. Intensive growth of UWB systems needs a deep understanding of the mechanisms leading to clutters due to rough surfaces or nonhomogeneous interfaces [10] which influence the spectral content of the response. Therefore, propagation and scattering wideband (quasi-noise) signals are becoming an important issue in design UWB systems operating in complex real world environments.

The paper is focused on formulating the criteria for application noise and coherent signals in microwave and mm-wave sensing as well as scattering from dense random media. In order to formulate such a criteria the double-layers dielectric structures is considered. It demonstrates typical oscillating pattern of transmission coefficient in frequency domain which originates from the Fabry-Perot effect. To create a transmittance interferogram the adjustable air gap between the two layers is introduced. The setups operating in W band (75–110 GHz) and 1–10 GHz band were assembled and tested with different nonhomogeneous materials (coal, wood chips, sand, and Teflon powder) in order to estimate the role of destructive factors in measurement microwave and mm-wave absorption using coherent and quasi-noise probing signals.

2. MODELING INTERFERENCE IN PRESENCE OF NOISE

Multi-layers plane-parallel dielectric structures are good candidates for estimating the roles of interference and noise averaging effects. Indeed, when the distance between layers is varied a spatial distribution of the interference maxima (minima) is taken place. A periodicity, swing and height of interference maxima (minima) depend on both real and imaginary parts of refractive index n and k (or complex dielectric constant $\varepsilon' = n^2 - k^2$, $\varepsilon'' = 2nk$). By recording the transmitted

signal we can easily compare interferograms for coherent and noise illuminating fields.

The configuration of a plane-parallel cell employed in the experiments described below is shown in Fig. 1. It consists of the two dielectric plates of thickness t separated by air gap L. Part of the transmitted energy is captured by wideband detector. In order to create a transmittance interferogram the variable air gap L is introduced.
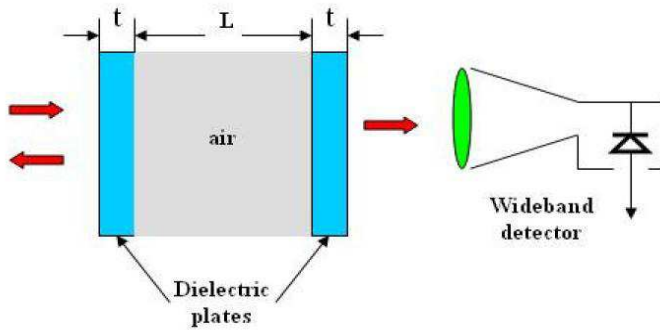

Figure 1. Configuration of the measuring cell used in mm wave experiments.

Assuming that the measuring cell is illuminated by plane wave we can calculate resulting transmittance matrix of the measuring cell T_c as a product of matrices describing separate layers [11], namely,

$$T_c = T_t \cdot T_L \cdot T_t \tag{1}$$

where:

$$
T_t = \begin{bmatrix} \cosh(\beta_t t) & \frac{i}{\sqrt{\varepsilon_{rt}}}\sinh(\beta_t t) \\ i\sqrt{\varepsilon_{rt}}\sinh(\beta_t t) & \cosh(\beta_t t) \end{bmatrix}
$$
$$
T_L = \begin{bmatrix} \cos(\beta_L L) & i\sin(\beta_L L) \\ i\sin(\beta_L L) & \cos(\beta_L L) \end{bmatrix}
\tag{2}
$$

$\beta_t = 2\pi\sqrt{\varepsilon_{rt}}/\lambda$, $\varepsilon_{rt} = \varepsilon'_{rt} - i\varepsilon''_{rt}$, $\beta_L = 2\pi/\lambda$.

Power transmittance T_p of the cell considered can be presented in the following form [12] taking into account its symmetry:

$$T_p = \left| \frac{2}{2T_{c(11)} + T_{c(12)} + T_{c(21)}} \right|^2 \tag{3}$$

where $T_{c(11)} = T_{c(22)}$, $T_{c(12)}$ and $T_{c(21)}$ are elements of transmittance matrix T_c.

Typical behavior of power transmittance as a function of distance L calculated using (3) at frequency $96.5\,\mathrm{GHz}$ is depicted in Fig. 2 for Al_2O_3 sample with $t = 2.19\,\mathrm{mm}$, $\varepsilon'_{rt} = 9.6$ and $\tan\delta = 0.001$. The behavior of power transmittance in frequency domain is shown in Fig. 3 for the distance between plates $L = 30\,\mathrm{mm}$.
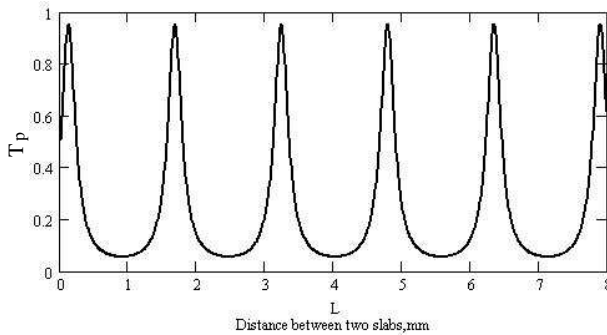

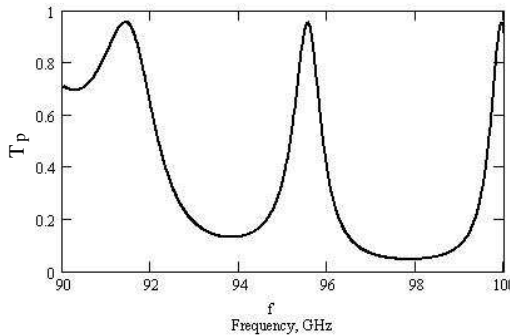**Figure 2.** Interferogram of the power transmittance as a function of distance L.

Figure 3. Interferogram of the power transmittance as a function of frequency f.

Interferograms depicted in Figs. 2 and 3 correspond to the coherent illumination of the dielectric plates. When probing signal is a frequency limited noise we need to introduce some assumptions:

1. Noise spectra occupies the band $f_c - BW/2$ to $f_c + BW/2$, where BW is the bandwidth of the frequency limited noise signal and f_c is the carrier frequency;

2. Power spectral density is uniform randomly distributed function within the specified BW.
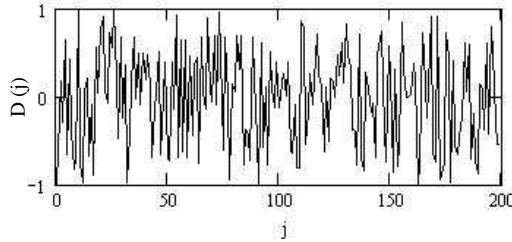
Figure 4. The example of normalized uniform random distribution of the 200 frequency components.

Following [10], the total averaged power transmittance T_{av} can be estimated from the following expression

$$T_{av} = \int_{f_c - BW/2}^{f_c + BW/2} T_p(f)D(f)df \qquad (4)$$

where $D(f)$ is the normalized spectral density distribution.

As an example, the tested $D(j)$ function of the unit amplitude is depicted in Fig. 4 for 200 frequency components randomly und uniformly distributed within the normalized bandwidth $\Delta\%$. The averaged transmittances power T_{av} of this distribution have been calculated from (4) by means of "injecting" in a carrier frequency f_c the frequency limited noise of bandwidth Δ varying in the range 2–100%. The random numbers generator has been used to imitate such an "injection". The results of calculations are shown in Fig. 5 where we can clearly observe that the periodicy of transmittance interferograms is degrading with increasing Δ. Beginning from the value of $\Delta = 30\%$ and more the noise averaged power transmittance tends to its weighted median value near $T_{av} = 0.45$.

3. MM-WAVE EXPERIMENTS

In order to verify a validity of the suggested model the mm-wave setup has been assembled for operating in W-band [13, 14]. It allows to record frequency limited incoherent transmittance interferograms using wideband pyroelectric detector and W-band noise source. The same experiments can be performed for coherent condition if the noise source is replaced by CW W-band source.

The schematic of the experimental setup is shown in Fig. 6. It consists of W-band coherent source (1) Millitech (model GDM-
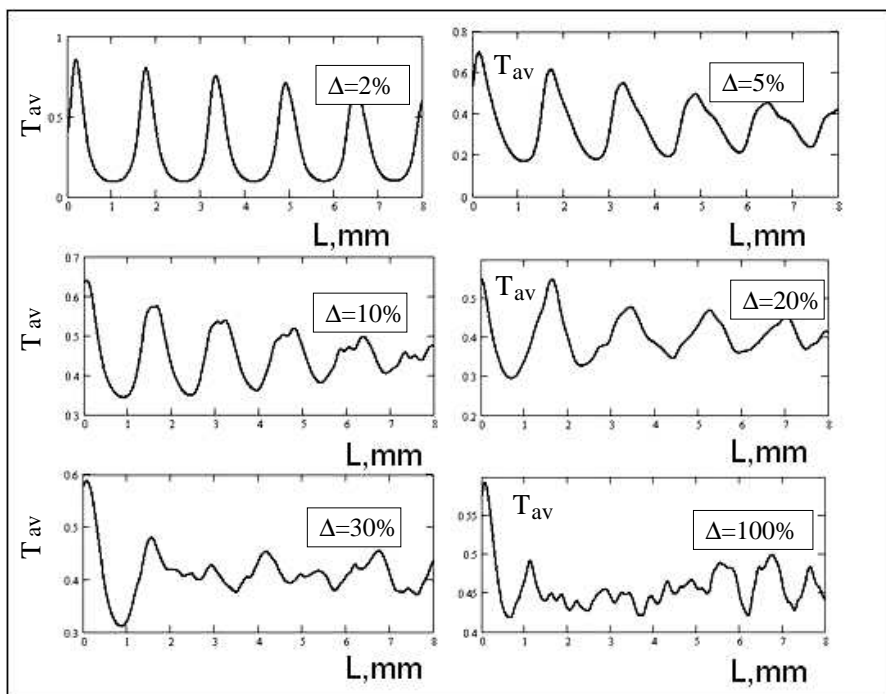
Figure 5. The calculated power transmittances corresponding to the distribution shown in Fig. 4 for different limited noise bandwidth Δ varying in the range 2–100%.
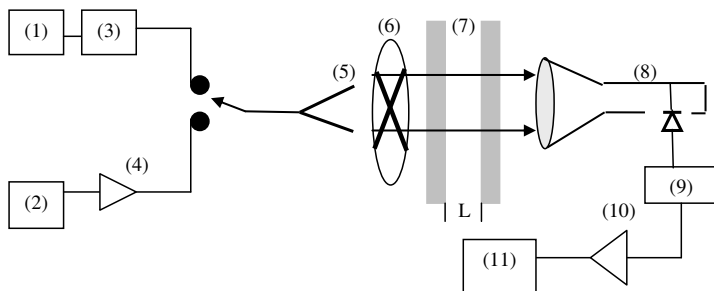

Figure 6. The schematic of the experimental setup operating in W-band.

10-3013M) and full W-band (75–110 GHz) noise source (2) Farran (model WG-NS-10) with ENR 13–15 dB. Since the output power of the coherent source is about 13 dBm a direct reading attenuator (3) is

added to avoid overloading of the pyroelectric detector (8) operating in the range 0.1–3.0 THz. On the other hand, the output power of the noise source is low in order to be directly measured by this detector. Therefore, W-band amplifier (4) is added at the output of the noise source. Both coherent and incoherent sources are connected alternately to the horn antenna (5) whose aperture is overlapping by rotating chopper (6) forming the AM modulation with frequency 10 Hz. The High-Performance Mid-Range Travel Linear Stage (the programmable micro-stepper), model ILS-100pp, Newport Co. is used for changing distance L between the two dielectric plates (7) with accuracy about $2\,\mu m$. The slabs of thickness $t = 2.19\,mm$ were fabricated from Al_2O_3. One of the plates is fixed while the second one is mounted directly on the input window of the detector so that both detector and the second plate are moving in longitudinal direction simultaneously varying the distance L between the dielectric plates. Transmitted energy comes to the input window of MICROTECH pyroelectric detector. The detected signal is filtered by BPF (9) with the central frequency $f = 10\,Hz$ (bandwidth = 1 Hz) and amplified by operational amp (10). The Tektronix digital scope (11) is used for recording the detected signal. The general view of W-band experimental setup is shown in Fig. 7.
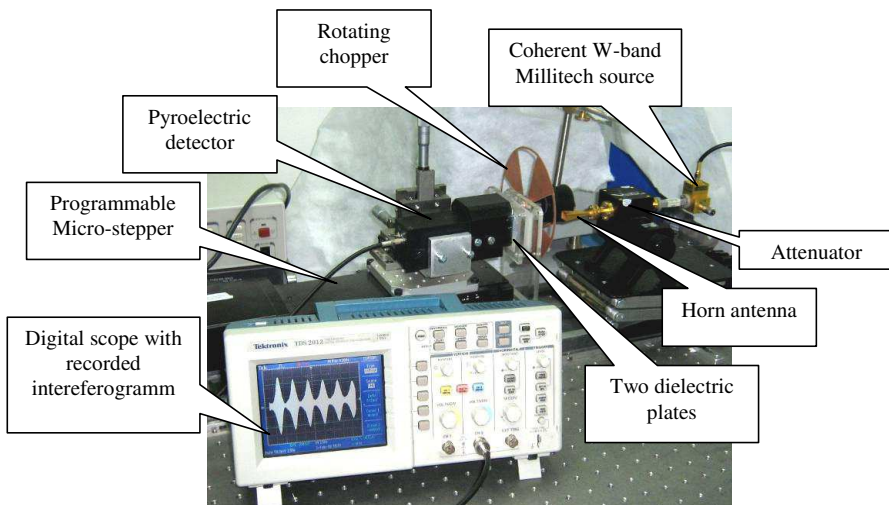

Figure 7. The general view of the W-band experimental setup with a coherent source.

First of all, the detector's output has been recorded as a function of distance when the source is switched off. The result of such experiment is shown in Fig. 8 and illustrates the own noise performance of the
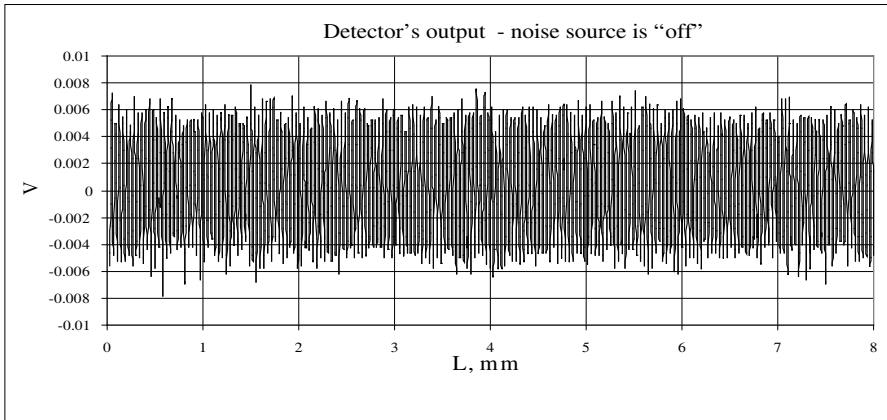
Figure 8. The recorded detector's output (in Volts) as a function of distance when the source is switched off.
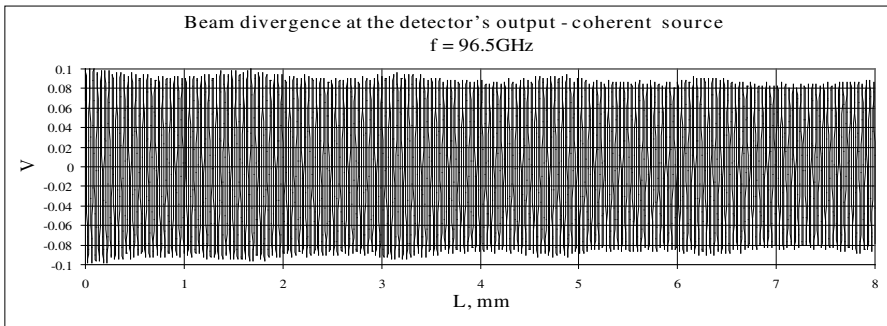

Figure 9. The recorded detector's output (in Volts) as a function of distance when the coherent source is switched on at frequency 96.5 GHz.

given setup. The average level of output noise does not depend on the distance L hence there are no additional external sources that can disturb transmittance measurements. Next, the coherent source was switched "on" at frequency 96.5 GHz and similar recording has been repeated with removed dielectric plates in order to estimate the beam divergence, Fig. 9. It is seen that the beam is rather uniform within the measured interval and the incident power can be assumed as a constant in calculations of power transmittance.

Then the two dielectric plates were installed and the coherent source was switched "on". Fig. 10 shows the measured transmittance interferogram as a function of the distance between the slabs for
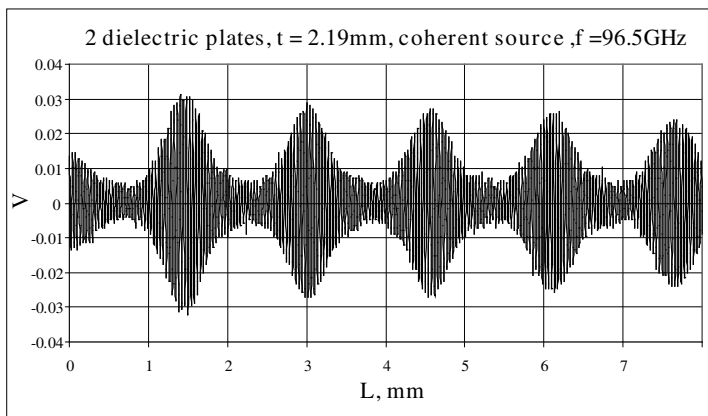
Figure 10. The detector's output (in Volts) as a function of the distance between the two dielectric plates for coherent illumination at frequency 96.5 GHz.
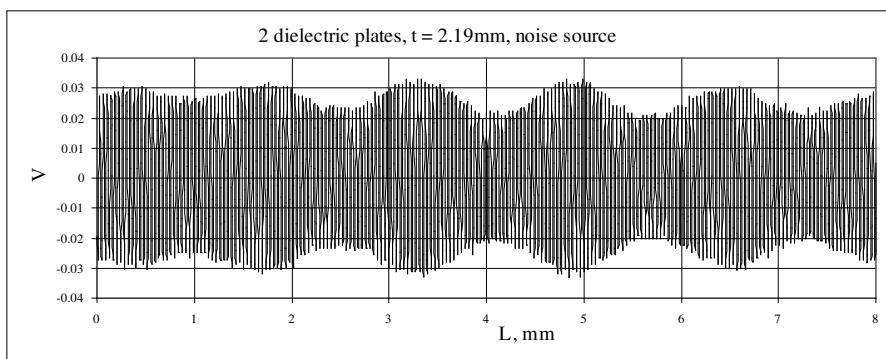

Figure 11. The detector's output (in Volts) as a function of the distance between the two dielectric plates for incoherent illumination.

coherent illumination at frequency 96.5 GHz. Similar measurements were performed with incoherent illumination for the same plates and shown in Fig. 11. It can be seen that the variation of a magnitude of the transmitted signal is more less in comparison with coherent mode proving the concept of noise averaging. It should be pointed out that accurate estimating real bandwidth of this setup is quite difficult since it needs knowledge of actual transfer functions of all components forming T_x and R_x channel (detector, LNA, antenna, etc.). We have assumed that system bandwidth 20–25% is quite realistic for the components used in the setup depicted in Fig. 7.

4. ANALYSIS AND DISCUSSION

As a first step in analysis of interferograms shown in Figs. 10 and 11, the standard median smoothing procedure has been applied to the absolute magnitude of the recorded signal. More fine structure of this signal's pattern can be reconstructed using Gaussian-kernel locally weighted averaging of the input data's vector vy' [16]. For each element in the n-element vector vy, the kernel smooth function returns a new vy' element given by:

$$vy'_i = \frac{\sum_{j=1}^{n} K(\frac{vx_i - vx_j}{b})vy_j}{\sum_{j=1}^{n} K(\frac{vx_i - vx_j}{b})} \text{ where } K(t) = 1.078 \exp\left(3.65t^2\right) \quad (5)$$

where b is a bandwidth which is supplied to the kernel smooth function. The bandwidth is usually set to a few times the spacing between data point on the x axis depending on how big a window we want to use when smoothing.

Final results of such reconstructions are depicted in Figs. 12 and 13 after normalizing to incident signals. We can clearly observe the quasi periodical structure of the transmittance pattern T_p inherent to coherent illumination as well as essential averaging effect typical for incoherent illumination. This effect leads to a reduction of the power transmittance variations in a vicinity of $T_{av} = 0.45$. That is quite close to the theoretical prediction obtained for the frequency-limited noise bandwidth $\Delta = 30\%$ shown in Fig. 5. It should be pointed out that the bandwidth of the noise source used in experiments is about 25% but operating bandwidth of the pyroelectric detector is
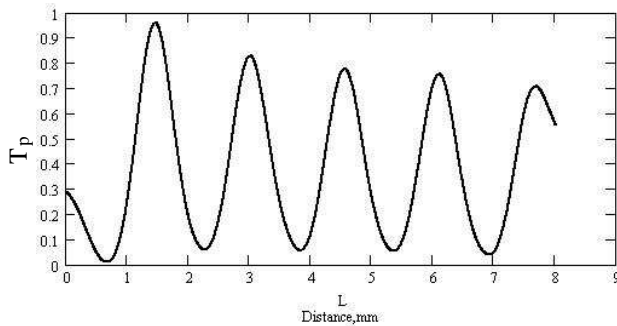

Figure 12. The reconstructed coherent interferogram based on Gaussian-kernel locally weighted averaging at frequency 96.5 GHz.
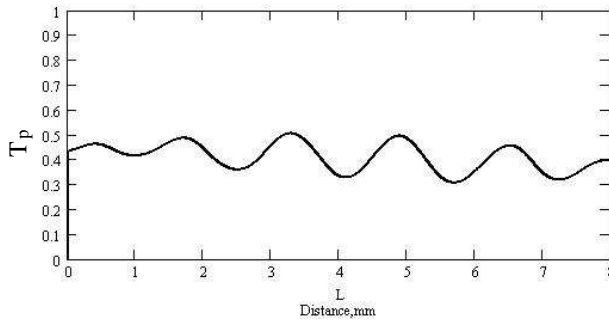
Figure 13. The reconstructed incoherent interferogram based on Gaussian-kernel locally weighted averaging, $\Delta = 25\%$.

much wider. On the other hand the input LNA limits real bandwidth of the transmitted channel. In fact, it is very difficult to estimate total transfer function of the transmitted channel including both LNA and noise source. Hence, within the above assumptions we can state out that criterion of "reasonable" averaging is $\Delta = 25\%$ of total noise bandwidth or even more.

Most of real world systems are more complicated than the two parallel dielectric slabs and interference of coherent signal may take place in a presence of curved surfaces too. Also, non-stable orientation of samples under tests moving on a conveyor belt in industrial conditions is a source of uncontrollable interference. Nevertheless, noise illumination may suppress undesirable interference inherent coherent mode too. As an example, a plastic container of height about 30 cm and diameter about 50 cm filled with Teflon powder has been illuminated by horn antenna connected with transmitter while receiver was connected with the same antenna as shown schematically in Fig. 14. The container (drum) was moving respectively antennas in transversal direction along the arrow.

Both the transmitted signals generated by the coherent source at frequency 100 GHz and the noise source (75–110 GHz) have been recorded as a function of a position of the container respectively the axis of antennas. This position is proportional to the sampling measurement numbers — horizontal axis on the plots. The envelopes of transmitted signals recovered after post-processing are shown in Fig. 15 for coherent (a) and noise (b) modes of illumination (A. Greenwald, private communication). The reference levels correspond to positions of container far from the axis of antennas when transmitted and received beams are in free space, namely, 1.1 V and 0.5 V for coherent and noise illuminations respectively. In process of moving the container
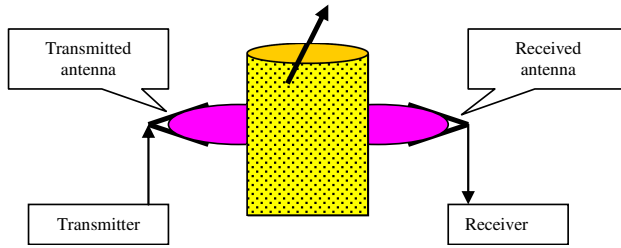
Figure 14. Plastic container (dram) with Teflon powder moving between transmitting and receiving antennas in transversal direction.
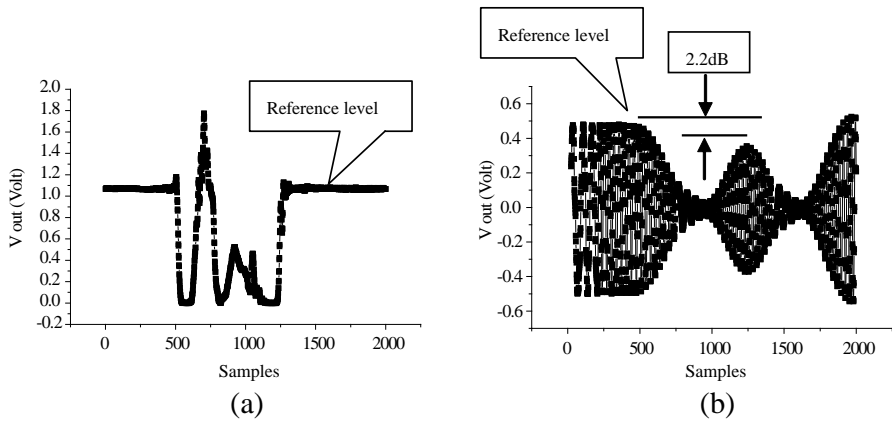

Figure 15. The envelopes of transmitted signals recovered after post-processing: coherent (a) and noise (b) sources of illuminations [16].

crosses the axis of antennas and maximum insertion loss is observed when the diameter of a container is aligning with the axis of antennas. Comparison both situations shows strong interference peaks (10–15 dB) in the case of coherent illumination and efficient suppressing this undesirable effect with noisy signal. Sometimes the transmittance in coherent mode for the specific dram's positions is greater than the reference level while the noisy mode experiment demonstrates regular variations of insertion loss with its maximum about 2.2 dB.

Widely used microwave moisture meters are based on strong correlation between insertion loss and water content in bulky materials under test. When size of particles of nonhomogeneous (granular) material is compared with the wavelengths depolarization effects may cause additional increasing forward scattering loss which drastically increases error in moisture content determination. In order to illustrate
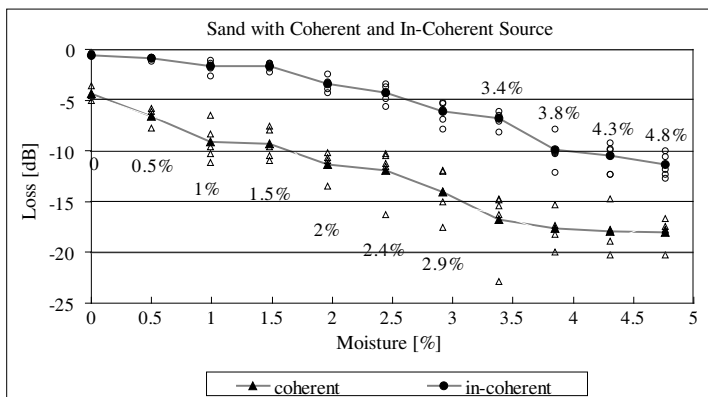
Figure 16. Measured insertion loss as a function of moisture content for coherent and incoherent illuminations. Thickness of the tested sample is 1 cm.

the role of this phenomenon the container filled with wet sand having preliminary known moisture content was illuminated both coherent and incoherent signals. The results of such measurements in W-band are shown in Fig. 16 for thickness of the sample 1 cm. Due to natural imperfections inherent sand samples the depolarization leads to additional increasing loss for coherent mode compared with incoherent one. Discrepancy in the measured loss is about 5–10 dB that is in principle unacceptable for accurate moisture determination. The similar effect has been reported in [15] where comparison coherent and noise illuminations were done also in microwaves range that is discussed in the next section.

5. MICROWAVE EXPERIMENTS

A variety of microwave systems are employed for on-line monitoring moisture content in bulk materials like coal, sand, wood chips, tobacco leafs and many others moving on conveyor belt. All of them are basically illuminated by coherent signals consisting of single or several frequency components. Sometimes a number of frequency components are 20 or more that is needed to improve averaging process. The basic drawback of coherent illumination is the parasitic depolarization effect leading to splitting radiated wave on the two components: co-polarized and cross-polarized [3]. As a result, additional losses of microwave energy provide contribution to the measured attenuation degrading accuracy of moisture determination since losses are function
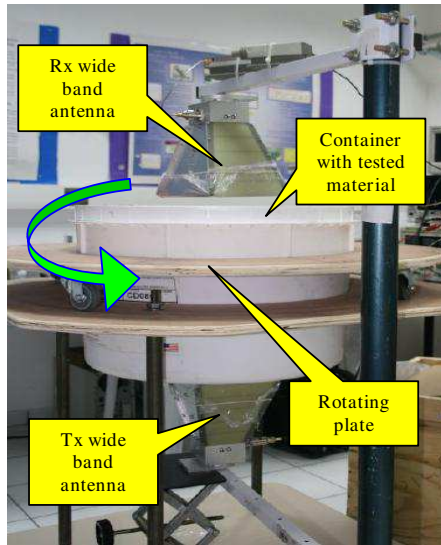
Figure 17. The experimental setup using rotating container filled with a material under test.
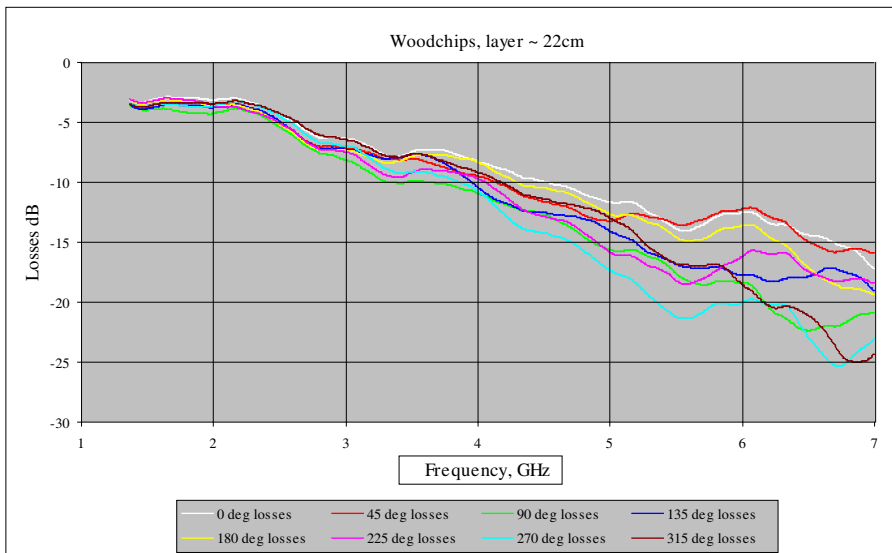

Figure 18. The measured insertion losses in coherent mode for wood chips (layer thickness 22 cm).

of moisture content. The roles of depolarization and destructive interference are more essential when an overall size of particles is compared with wave length.

In order to simulate real-world vibrations and variations of thickness on the conveyor belt, the container with material under test is rotated as depicted in Fig. 17. Since the experiments are performed in wide frequency range, the wide band horn-ridged R_x and T_x antennas are used both in the coherent and noisy modes.

The calibration of the setup has been done independently for coherent and noise modes of operation. The Agilent vector network analyzer PNA-L N5230C was used for measurements in the coherent mode. The noise source operating in 1–8 GHz with noise integrating detector were applied for the noisy mode. Insertion losses of three types of nonhomogeneous materials have been measured: wood chips, coal and sand. Typical results of measurements in coherent mode are shown in Figs. 18–20. The container with material under test was rotated 0°–360° with the step 45° in order to imitate instability taken place in reality. Variations of insertion losses are small at frequencies less than 2 GHz and increases toward higher frequencies for all materials since wavelength is becoming comparable with size of particles. This tendency proves important role of particles size
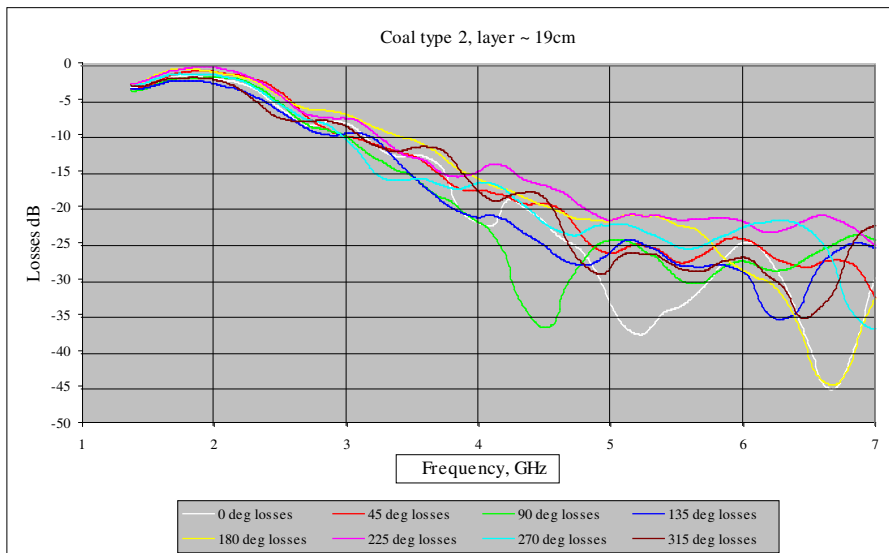

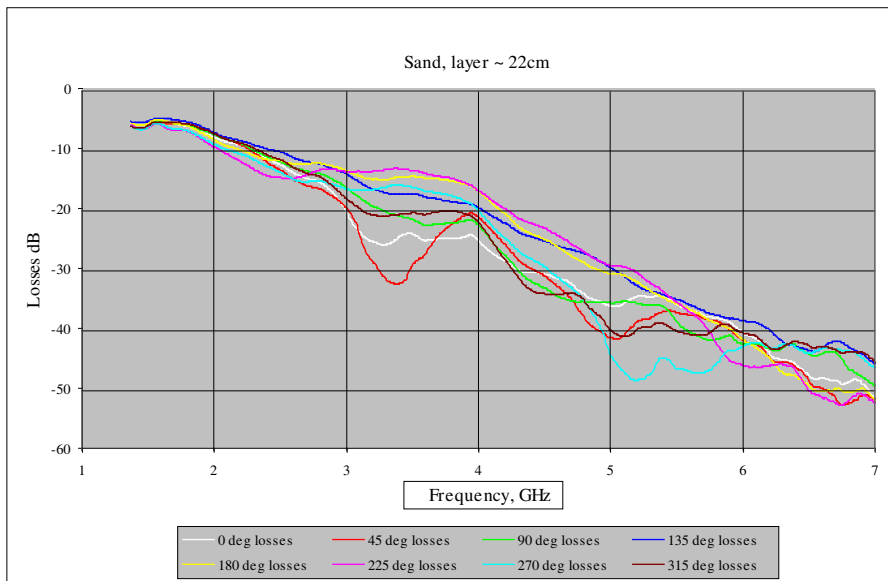**Figure 19.** The measured insertion losses in coherent mode for coal (layer thickness 19 cm).

Figure 20. The measured insertion losses in coherent mode for wood chips sand (layer thickness 22 cm).
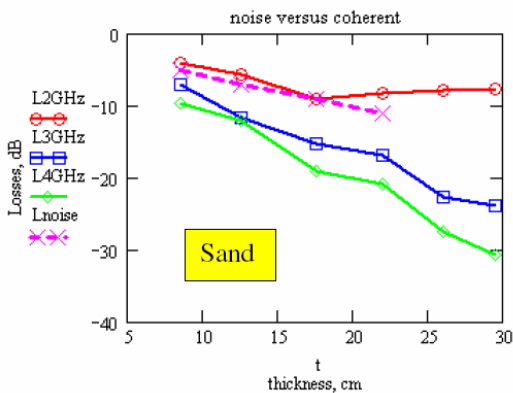

Figure 21. The averaged values of insertion losses as a function of thickness of the sand's layer.

compared with wavelength regardless of the type of material under test.

In order to estimate the effect of interference the measurements were performed with several layer's thicknesses. The averaged values
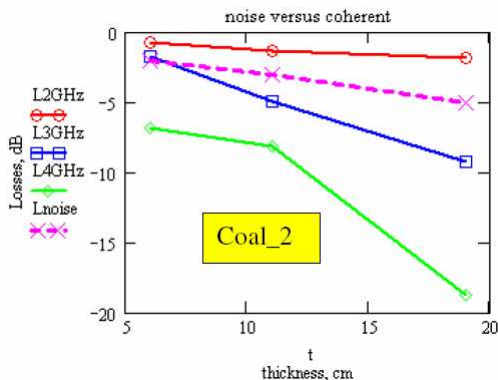
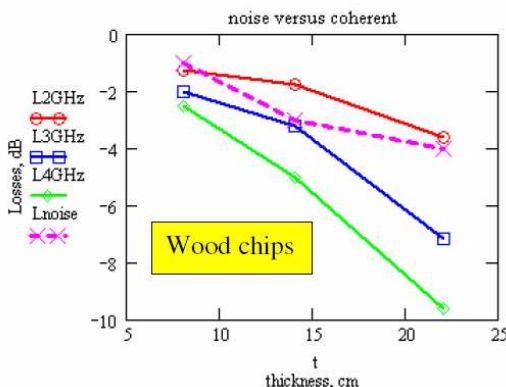**Figure 22.** The averaged values of insertion losses as a function of thickness of the coal's layer.

Figure 23. The averaged values of insertion losses as a function of thickness of the wood chips layer.

of insertion losses for all samples rotated with the step 45° (8 measurements) are depicted in Figs. 21–23 for specified frequencies 2, 3 and 4 GHz using coherent illumination. Similar testing was performed with noise illumination shown by mark x-x-x at the same figures. The following averaged sizes of particles were used in experiments: 3–8 cm(coal), 1–5 cm (wood chips) and 0.01–0.1 cm (sand). All the experiments with the coherent mode have demonstrated 2–3 times greater variation of insertion loss at frequencies higher 4 GHz compared with the noise mode. This effect becomes more essential with increasing thickness of the tested material. However, if attenuation in bulky material is too high due to increased moisture content, for

Table 1. Comparison of the maximum variation of transmission for coherent and noisy illuminations in percents.

Material	Coherent illumination	Noisy illumination
Sand	40.4	20.6
Coal 1	74	30.769
Coal 2	238.9	100
Wood chips	75.594	36.364

example, uncertainty caused by variation of thickness may be decreased since interference and depolarization effects in lossy medium have a tendency to be smoothed.

Finally, the Table 1 summarizes a comparison of the maximum variation of transmittance in percents for coherent and noisy illuminations. The noise illumination has demonstrated about 2 times less variations of the measured transmission compared with coherent mode for all the tested materials.

6. CONCLUSION

Based on modeling and experiments it was found out that the "good-of-fit" confidence bandwidth of the frequency limited noise is about 25% of the CW carrier frequency. This value is recommended as a criterion of noise versus coherency competition in mm waves and microwave characterizations of nonhomogeneous materials. If the bandwidth of quasi-noise signal is less than above value the noise and coherent modes may demonstrate similar results in estimating insertion losses (or forward scattering experiments). However, it is not the absolute conclusion since real sizes of particles may add corrections to the above criterion as well as specific conditions of experiments must be taken into account. Anyway, use of the noise illumination allows reducing variations of insertion losses 2 times or more depending on a type of material.

REFERENCES

1. Chen, L. F., C. K. Ong, C. P. Neo, V. V. Varadan, and V. K. Varadan, *Microwave Electronics — Measurement and Materials Characterization*, John Wiley, 2004.

2. Koh, G., "Experimental study of electromagnetic wave propagation in dense random media," *Waves in Random Media*, Vol. 2, 39–49, 1991.

3. Toropainen, A. P., "New method for measuring properties of nonhomogeneous materials by a two-polarization forward-scattering measurement," *IEEE Trans. MTT*, Vol. 41, No. 12, 2081–2086, 1993.

4. Sihvola, A., "Electromagnetic mixing formulae and applications," *IEEE Electromagnetic Waves Series*, Vol. 47, 2004.

5. Kandala, C. V. and J. Sundaram, "Nondestructive measurement of moisture content using a parallel-plate capacitance sensor for grain and nuts," *IEEE Sensors Journal*, Vol. 10, No. 7, 1282–1287, 2010.

6. Trabelsi, S., and S. O. Nelson, "Microwave sensing technique for nondestructive determination of bulk density and moisture content in unshelled and shelled peanuts," *Transactions of the ASABE*, Vol. 49, No. 5, 1563–1568, 2006.

7. Li, Z., A. Sharma, A. I. M. Ayala, M. N. Afsar, and K. A. Korolev, "Broadband dielectric measurements on highly scattering materials," *IEEE Trans. IM*, Vol. 54, No. 5, 1397–1405, 2010.

8. Polivka, J., P. Fiala, and J. Machac, "Microwave noise field behaves like white light," *Progress In Electromagnetics Research*, Vol. 111, 311–330, 2011.

9. Kapilevich, B., B. Litvak, T. Ben Yehuda, and O. Shotman, "Comparative characteristics of coherent and incoherent microwave scattering in dense inhomogeneous layers," *Russian Physics Journal*, Vol. 49, No. 9, 913–916, 2006.

10. Ghavami, M., L. B. Michael, and R. Konho, *Ultra Wideband Signals and Systems in Communication Engineering*, John Wiley & Sons, 2004.

11. Cornbleet, S., *Microwave and Geometrical Optics*, Academic Press, 1994.

12. Pozar, D., *Microwave Engineering*, 3rd edition, John Wiley & Sons, 2005

13. Kapilevih, B. and B. Litvak, "THz characterization of high

dielectric-constant materials using double-layer sample," *Microwave and Optical Technology Letters*, Vol. 49, No. 6, 1388–1391, 2007.

14. Kapilevich, B. and J. Polivka, "Noise versus coherency in mm-wave material characterization," *The 33rd International Conference on Infrared, Millimeter, and Terahertz Waves*, Paper ID#1139, California Institute of Technology, Pasadena, California, USA, 2008.

15. Polivka, J., "An overview of microwave sensor technology," *High Frequency Electronics*, Vol. 6, No. 4, 32–42, 2007.

16. Mathcad Professional, "Smoothing of X-Y data by Kernel smoothing," *Data Analysis Documentation*, 2001.